Compact Modeling of MEMS Contact Current upon Pull-In

H. I. Røst[1], J. V. Clark[2], K. S. J. Pister[3]

[1]Norwegian University of Science and Technology, Norway
[2]Auburn University, USA
[3]University of California at Berkeley, USA

ABSTRACT

This work-in-progress presents a parameterizable compact model of a microelectromechanical system (MEMS) beam element that includes mechanical contact and electrical current flow upon gap closure. Quasistatic electromechanical simulation analyses include the initial onset of pull-in followed by an increase in surface contact as voltage and current continue to increase. The traditional beam element without contact is a key building block for many types of MEMS. However, by adding mechanical and electrical contact physics to the beam model, then the computationally-efficient design and simulation of many other types of MEMS that experience contact may be explored. Prior efforts by others include closed-form pull-in analytical models and simulations of pull-in and lift-off without electrical contact. We describe our compact model and simulate the characteristic behaviors of a simple gap-closing actuator and a zipper actuator with dimples.

Keywords: pull-in, compact model, lumped model, contact current

1 INTRODUCTION

The compact model of the beam element has been used to model a large variety of MEMS devices that do not experience contact [1-3]. However, there are plenty of MEMS devices that undergo contact. Examples include RF MEMS switches or relays, analog to digital converters, low-power potential energy stores, mechanical memory, gap stops, high-acceleration impact, torsional switches or micromirror (e.g. digital light processing (DLP)), vertical diffraction gratings, zipping actuators, lateral comb drive instability, etc.

Prior efforts to model contact include closed-form pull-in analytical models [4-6], simulations of pull-in and lift-off without electrical contact [7-9], and the modeling of separate gate/drain pull-in switches [10-11]. A comprehensive review of electrostatic pull-in instability is given in [12]. To our best knowledge, a compact model of contact current of the gate electrode upon pull-in has not

been reported. Our parameterized compact model includes an electrostatic attractive force for pull-in, a short-range repulsive force to prevent beam elements from passing through each other, the spring force, and a simple current source that is switched on when the gap closes. Once closed, current flows between the pair of touching beam elements.

In Section 2, a description of our compact model and simulation method are presented; and in Section 3, the characteristic behaviors of a gap-closing actuator and a zipping actuator with dimples are simulated as test cases.

2 PULL-IN CONTACT MODEL

In this section we present our mechanical contact model followed by our electrical contact model. The three types of forces considered for pull-in are the attractive capacitive force, repulsive spring force, and repulsive contact force:

$$F_{capacitor} = \frac{1}{2} \frac{\varepsilon L h}{\left(gap_0 - x \right)^2} V^2$$

$$F_{spring} = - K x$$

$$F_{contact} = - \frac{B}{\left(gap_0 - x \right)^7} \tag{1}$$

$$F_{net} = F_{capacitor} + F_{spring} + F_{contact}$$

where K is the stiffness of the spring supporting the gap plate, x is the displacement of the plate, gap_0 is the initial gap distance between the two plates of the capacitor at zero state, ε is the permittivity of the medium, Lh is the facing area of the plate, and V is the voltage difference between the plates. Our contact force is similar to Lennard-Jones repulsion. We have chosen to set the constant B using the boundary condition at gap closure. Gap closure is at a displacement of $x_0 = gap_0 - h_R$, where h_R is the thickness of a resistive layer on the plate. Upon closure, the net force goes to zero as $x \to x_0$. Therefore, the constraint on B is

$$B = \left[\frac{1}{2} \frac{\varepsilon L h}{\left(gap_0 - x_0 \right)^2} V^2 - K x_0 \right] \left(gap_0 - x_0 \right)^7. \tag{2}$$
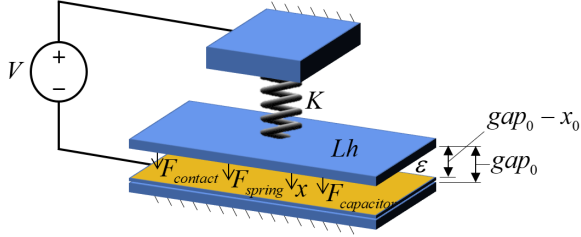
Figure 1: The configuration of the canonical pull-in model in (1). The arrows indicate the positive sense for the respective quantities of force and displacement.
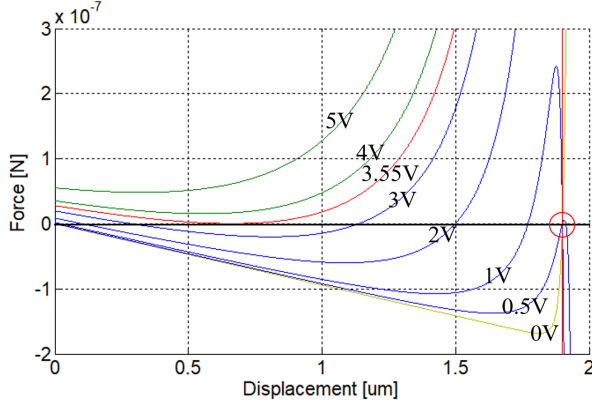

Figure 2: Force vs. displacement from zero-state to gap-closure of Equation (1). A positive net force is attractive here. Due to (2), the net force is zero at gap closure, $x = 1.9\mu m$.

This constraint enables the plate to achieve a consistent contact position upon pull-in, independent of voltage.

Figure 1 shows the configuration of the canonical model in (1), where a pair of conductive plates are separated by a gap. The upper conductive plate is supported by a conductive spring, and a resistive layer has been deposited on the lower conductive plate.

To examine how contact works in this model, let's use the following quantities: $gap_0 = 2\mu m$, $x_0 = 1.9\mu m$, $K = 0.094$N/m, $Lh = 100\mu m \times 20\mu m$, $\varepsilon = 8.854 \times 10^{-12}$ F/m. Given a variety of applied voltages ranging from 0V to 5V, as seen in **Figure 2**, the net force is attractive at all gap locations for voltages at or above the pull-in voltage of 3.553V. For verification, the pull-in formula gives $V_{PI} = \sqrt{8Kg_0^3/(27\varepsilon Lh)} = 3.547$V, having a 0.1% error that is likely due to iteration step-size error. For voltages below the pull-in voltage, the net force changes from being attractive near zero-state, repulsive at intermediate states, attractive near gap-closure, and repulsive beyond gap-closure. Locations of zero net-force correspond to equilibrium states as shown in **Figures 3**. Verification of mechanical contact is shown in **Figure 4**, where the gap remains closed as voltage continues to increase beyond pull-in.
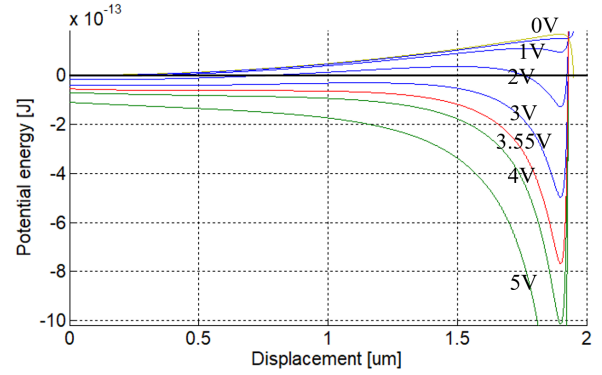

Figure 3: Potential energy $U_{capacitor} + U_{spring} + U_{contact}$ of (1), plotted as a function of displacement and applied voltage. The minima are stable points of equilibrium. For V > 0, the stable equilibrium at closure are all located at $x = 1.9\mu m$.
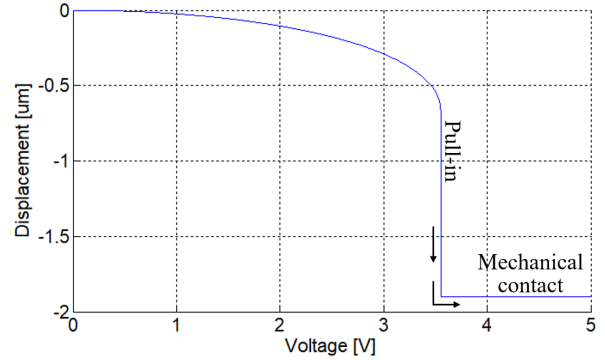

Figure 4: Quasi-static simulation of the pull-in and mechanical-contact of (1) as voltage is increased from 0V to 5V. Pull-in occurs at 3.55V, and the equilibrium displacement remains at $x = 1.9\mu m$ as voltage increases.

We model contact current as a multi-stage switch that depends on contact orientation. Our compact beam element model consists of lumped electromechanical end nodes [1], where forces, moments, voltages, displacements, and currents are accounted for. Due to this limitation, lumped models do not contain the finer details of distributed models. Each beam element is mechanically flexible and electrically conductive. Depending on the structural behavior, a beam element may make partial or full contact, affecting contact resistance. This situation is depicted in **Figure 5**, where an initial edge contact is followed by full contact. The type of contact abruptly affects both voltage and current.

Our quasi-static algorithm solves a system of the form

$$\begin{bmatrix} x \\ V \end{bmatrix} = \begin{bmatrix} K & 0 \\ 0 & G \end{bmatrix}^{-1} \begin{bmatrix} F(x,V) \\ I(x,V) \end{bmatrix} \qquad (3)$$

where K is the stiffness matrix [1], G is the conductance matrix, x is the displacement at each node, V is the voltage
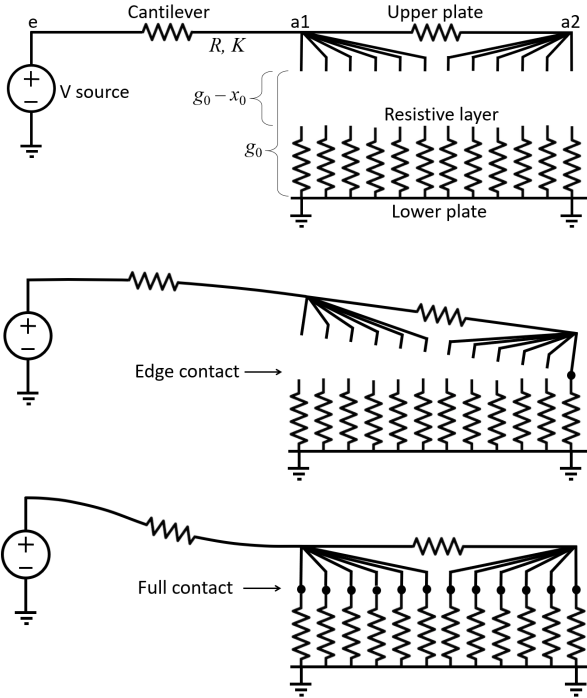
Figure 6: Progression of states through pull-in using our compact model. The node voltages and displacements are given for each state, where a source voltage is applied at node e. State A: a state of deflection immediately prior to partial pull-in at V_{PI} = 2.14V.. State B: partial pull-in where current flows through the elements. State C: after full pull-in as more current flows across the gap.

Figure 5: (a) Prior to contact: voltages at nodes a1, a2, and e are equal, and no current flows. (b) Edge contact: minimal current flows from the upper plate to the lower plate. (b) Full contact: maximal current flows between the plates.

at each node, F (electrostatic and contact) is the externally applied force vector depending of node displacements and voltages, and I (contact) is the externally applied current vector, being a discrete function of node displacements and voltages. That is, upon edge contact ($x_{a2} \rightarrow x_0$), the applied current at node a2 is $I_{a2} = V_{a2}G_{edge}$. At full contact, the applied current is $I_{a2} = V_{a2}G_{full}$, where G_{full} is the full conductance for all nodes opposite and contacting across the gap. Otherwise, when the gap is open, no current flows across the gap. Within our quasi-static (Newton solver) loop, the solution vector and sources $F(x,V)$ and $I(x,V)$ are updated for each applied voltage step.

3 SIMULATED EXAMPLES

In this section we use a compact model based on (1) to demonstrate the instability of pull-in, mechanical contact, and electrical contact. The model for the gap-closing element has the added ability to rotate as well as translate as the gap closes.

As shown in **Figure 6**, a simple gap closing actuator is simulated with an anchor, a supporting cantilever element, and a gap-closing element. The progression of three states is shown as increasing voltage is applied at the anchor node e to close the gap. A continuum of quasi-static states is shown in **Figure 7**, where the displacements of nodes a1 and a2 are plotted as a function of applied voltage at node e.
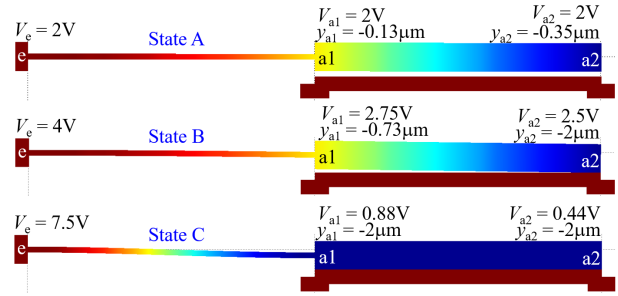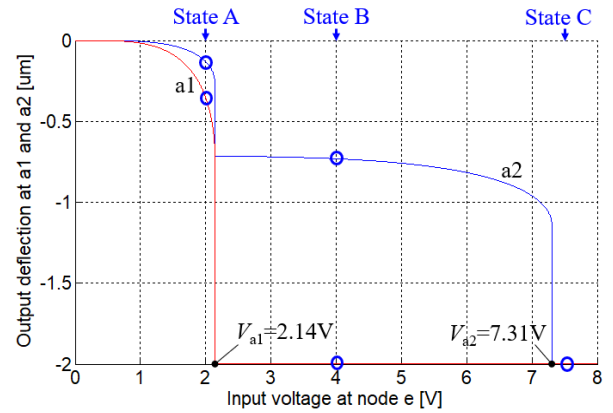

Figure 7: Simulation of deflection vs. input voltage. A continuum of quasi-static states for the device from Figure 6 is shown. An input voltage ranging from 0V to 8V is applied at node e. The deflections of nodes a1 and a2 are plotted from before to after gap closure. The locations of states A, B, and C in Figure 6 are circled.
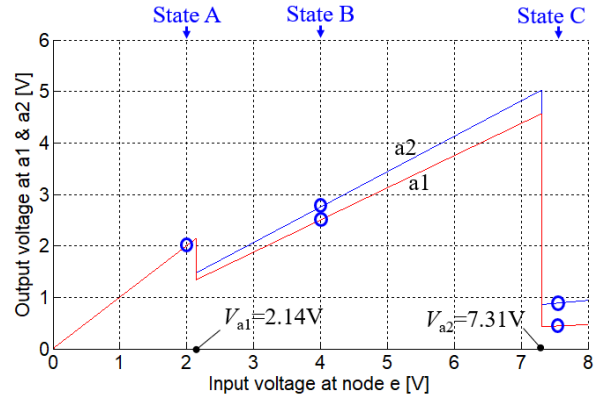

Figure 8: Simulation of output voltage at nodes a1 and a2 versus input voltage at node e. Abrupt voltage drops occur upon edge and full contact events. The slopes of input to output voltages change from 1 to lower ratios after contact current begins to flow.

The most flexible node a2 pulls in at 2.14V, followed by node a1 at 7.31V. If the gap element was constrained from rotation, the pull-in voltage would be 3.3V.
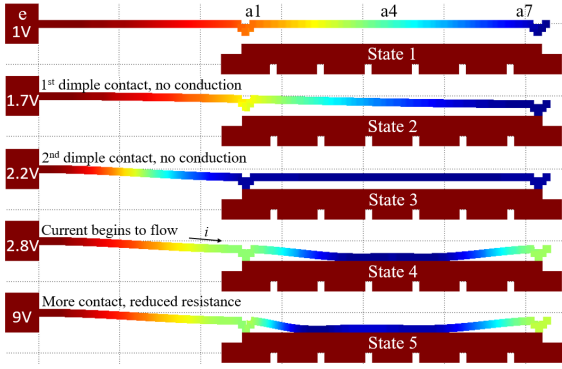
3

Figure 9: Progression of states through dimple-contact and zipper pull-in. Applied voltages at node e are indicated. $Gap_0 = 4\mu m$.
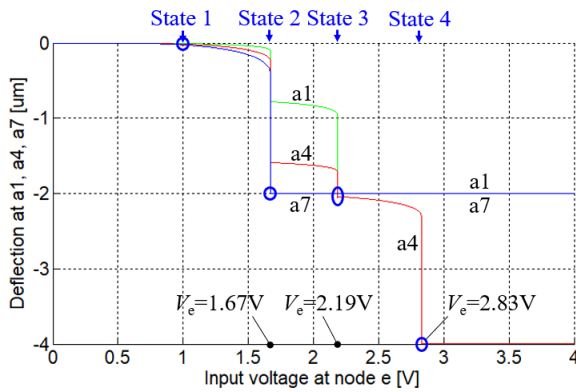

Figure 10: Plot of deflection at nodes a1, a4, and a7 versus input voltage at node e of the structure shown in Figure 9.

As the node a2 makes contact, the resistive element causes a voltage drop across the gap, accompanied by a flow of current. As node a1 is pulled in, full contact is achieved, causing a larger voltage drop and greater current flow. The trajectory of voltage ramps and drops are plotted in **Figure 8**, with three indicated states corresponding to those in **Figures 6** and **7**. The modeling parameters of the device are: cantilever length $L = 100\mu m$, width $w = 2\mu m$, layer thickness $h = 2\mu m$, sheet resistance $R_s = 10\ \Omega/sq$; and gap length $L = 100\mu m$, $w_1 = 10\mu m$, $w_2 = 5\mu m$, $h = 2\mu m$, $gap = 2\mu m$, $R_s = 10\Omega/sq$; and gap resistance $R_{gap} = 100\Omega$.

As a second example, the gap model is extended to represent a dimple that does not conduct upon closure by eliminating the gap model's contact current source. A distributed electrode is formed by connecting six gap elements in series (node a1 to a2, a2 to a3 etc.). Five simulated states are shown in **Figure 9** for increasing voltages at node e. The dimples make contact at States 2 and 3 with no current flow. Between States 4 and 5 the electrode pulls in, increasing its surface contact area and current across the gap. The zipped pull-in is asymmetric because voltage is higher on the cantilever side. Deflections of nodes a1, a4, and a7 are plotted as a function of applied voltage at node e in **Fig. 9**.

4 CONCLUSION

This work-in-progress explored the modeling and quasi-static simulation of a gap-closing element. The compact model demonstrated an ability to achieve stable mechanical contact upon gap closure, with and without electrical conductivity. At the point of contact, spring (~gap) and electrostatic (~gap^{-2}) forces were balanced against contact forces (~gap^{-7}), while a finite-state current source (~V) operated across the gap to model current flow.

REFERENCES

[1] J. V. Clark, K. S. J. Pister, "Modeling, Simulation, and Verification of an Advanced Microdevice Using Sugar," Journal of Microelectromechanical Systems, pp. 1524-1536, Aug (2007).

[2] J. E. Vandemeer, Nodal Design of Actuators and Sensors (NODAS), M.S. Thesis, Carnegie Mellon University, (1998).

[3] Tamara Bechtold, Gabriele Schrag, Lihong Feng, Oliver Brand, Gary K. Fedder, Christofer Hierold, Jan G. Korvink, Osamu Tabata, "System-level Modeling of MEMS", Wiley-VCH (2013).

[4] A. H. Nayfeh, M. I. Younis, E. M. Abdel-Rahman, "Dynamic pull-in phenomenon in MEMS resonators", Nonlinear Dynamics, Vol. 48, pp. 153-163, (2007).

[5] W. Yu, S. Gao, Y. Lin, M. He, L. Liu, J. Xu, Y. Luo, X. Cai, "MEMS-Based Tunable Grating Coupler", Photonics Technology Letters IEEE, vol. 31, no. 2, pp. 161-164 (2019).

[6] Z. Zhang, M. Kamon, L. Daniel, "Continuation-Based Pull-In and Lift-Off Simulation Algorithms for Microelectromechanical Devices", Journal of Microelectromechanical Systems," Vol. 23, Issue: 5, pp. 1084-1093 (2014).

[7] E. M. Miandoaba, H. N. Pishkenarib, A. Meghdarib, M. Fathic, "A general closed-form solution for the static pull-in voltages of electrostatically actuated MEMS/NEMS, Physica E, Vol. 90, pp. 7–12 (2017).

[8] H. Jaafar, O. Sidek, A. Miskam, S. Korakkottil, "Design and Simulation of Microelectromechanical System Capacitive Shunt Switches", American J. of Engineering and Applied Sciences, Vol. 2, No. 4, pp. 655-660 (2009).

[9] M. Kamon, S. Maity, D. DeReus, Z. Zhang, S. Cunningham, S. Kim, J. McKillop, A. Morris, G. Lorenz, L. Daniel, "New Simulation and Experimental Methodology for Analyzing Pull-In and Release in MEMS Switches", Transducers 2013, June (2013).

[10] Z. J. Guo, N. E. McGruer and G. G. Adams, "Modeling, simulation and measurement of the dynamic performance of an ohmic contact, electrostatically actuated RF MEMS switch", J. of Micromechanics and Microengineering, Vol. 17, pp. 1899–1909, (2007).

[11] A. Granaldi, P. Decuzzi, "The dynamic response of resistive microswitches: switching time and bouncing," J. of Micromechanics and Microengineering, Vol. 16, pp. 1108-1115, (2006).

[12] W.-M. Zhang et al, H. Yan, Z.-K. Peng, Guang Meng, "Electrostatic pull-in instability in MEMS/NEMS: A review", Sensors and Actuators A: Physical, pp. 187–218 (2014).